Lab on a Chip

PAPER

View Article Online
View Journal | View Issue

Cite this: *Lab Chip*, 2022, **22**, 4129

High sensitivity label-free detection of HER2 using an Al–GaN/GaN high electron mobility transistor-based biosensor

Shivanshu Mishra, *[ab] Pharyanshu Kachhawa, [ab] Amber Kumar Jain, [a] Rajiv Ranjan Thakur [ab] and Nidhi Chaturvedi[ab]

This work reports rapid, label-free and specific detection of the HER2 antigen using a gallium nitride (GaN) high electron mobility transistor (HEMT). Thiol-based chemistry has been utilized to immobilize the corresponding HER2 antibody in the sensing area of the sensor. The formation of a gold–sulfur complex has been confirmed through Raman spectroscopy, giving a peak at around a wavelength of 260 cm^{-1}. Fourier transform infrared spectroscopy and atomic force microscopy (AFM) also reveal the functionalization of thiol and free carboxylic groups. On-chip enzyme-linked immunosorbent assay has been utilized to confirm immobilization of antibody receptors on the sensing area surface, followed by current–voltage measurement. Morphology of the sensing area using AFM and electrical characterization of the sensor have been recorded before and after each functionalization process step. The sensor shows detection of the HER2 antigen in a broad range of 0.7 pg ml^{-1} to 10 μg ml^{-1} *i.e.*, (5×10^{-15} to 6×10^{-8} M). A long-time study and reusability aspect of the sensor have also been investigated that show good viability of the sensor. For the first time, a three-binding-site model based on the Langmuir isotherm has been developed for HER2 detection using GaN-HEMTs with three dissociation constants, *i.e.*, 7×10^{-10}, 8.8×10^{-11}, and 7.2×10^{-9} M, respectively.

Received 14th April 2022,
Accepted 26th August 2022

DOI: 10.1039/d2lc00349j

rsc.li/loc

1 Introduction

Human epidermal growth factor receptor 2 (HER2) is a transmembrane protein with tyrosine kinase activity involved in the normal growth and differentiation of epithelial cells.[1,2] The extracellular domain (ECD) of HER2 can be cleaved from the surface of cancer cells by matrix metalloproteases and released into the serum.[3] The ECD of the HER2 released in the blood served as an indicator of the overexpression of the HER2 antigen that can be detected using a monoclonal antibody.[4,5] Increased levels of HER2 (≥15 ng mL^{-1}) can be detected in approximately 15 to 30% of unselected presurgical breast carcinoma samples and in up to 45% of patients with metastatic breast cancer.[5,6] The overexpression of HER2 is not only limited to breast cancer but also found in various other human cancers such as non-small cell lung cancer (NSCLC) (10 to 30%),[7] salivary gland cancer (20%),[8] gastric or stomach cancer (10 to 30%),[9] esophageal cancer (10 to 50%),[10] ovarian cancer (20 to 30%),[11] and endometrial cancer (14 to 50%).[12] HER2 testing is commonly carried out by various diagnostic techniques such as enzyme-linked immunosorbent assay (ELISA),[13] immunohistochemistry (IHC)[14] and fluorescence *in situ* hybridization (FISH).[15] However, these detection techniques are fraught with labour-intensive, time-consuming methods and false negative results and require labels, a strict environment, and sophisticated instrumentation to carry out HER-2 detection.[16–18] Besides that, these methods require biopsy, an extremely invasive method that carries many risks. These hurdles make the widespread and frequent diagnosis of HER2 highly inconvenient, resulting in delayed diagnosis. These limitations urgently demand the development of less invasive, simple and low-risk methods suitable for point-of-care (POC) diagnosis of HER2 levels. Combining the knowledge of cancer biology, molecular targeting, and nanotechnology can enable the design of portable or hand-held devices for diagnosis, monitoring, and treatment of cancer appropriate for community or field use.[19] Gallium nitride (GaN)-based heterostructure FETs (HFETs), also known as high electron mobility transistor (HEMTs), provide high sensitivity and biocompatibility for biosensing applications due to their stability in chemically harsh and high-temperature environments.[20,21] The two-dimensional electron gas (2DEG) channel formed at the interface of AlGaN/GaN is very close to the surface and extremely sensitive to the surface charges.[22] The high sensitivity of GaN HEMTs towards surface charges facilitates a low-level detection of the

[a] *CSIR – Central Electronics Engineering Research Institute, Pilani, Rajasthan, India. E-mail: shivanshuceeri@gmail.com, shivanshumishra@ieee.org, nidhi@ceeri.res.in*
[b] *Academy of Scientific and Innovative Research, Ghaziabad, Uttar Pradesh, India*

HER2 antigen, which is the primary requirement for early-stage detection. Besides, these sensors also have a small size and low cost and only need a small quantity of test samples, thanks to the matured semiconductor microfabrication techniques. GaN HEMTs have been extensively used for pH detection with and without gate structures.[23,24] Nanorod-functionalized and 3-aminopropyltriethoxysilane (APTES) functionalized HEMTs have been used to detect glucose, with the enzyme glucose oxidase located on the sensing area.[25] Antibody driven PSA is detected at low concentrations using Au-gated Al–GaN/GaN HEMTs with a detection limit of 10 pg ml^{-1}.[26] The kidney injury molecule-1 (KIM-1) antigen has been detected using a GaN HEMT with an LOD of 1 ng ml^{-1}.[27] Sarangadharan *et al.* have successfully detected cardiac troponin-I with antibody immobilized extended gate GaN HEMTs with an LOD of 250 fM.[28] Hee Ho Lee *et al.* utilized GaN HEMTs for specific detection of C-reactive protein (CRP) using thiol-based chemistry on the gate area with an LOD of 0.1 ng ml^{-1}.[29] Ubiquitin carboxy-terminal hydrolase L1 (UCH-L1), also known as BA0127, is a promising biomarker for traumatic brain injury (TBI) and has been detected by antibody-functionalized GaN HEMTs. However, the LOD of the sensor is 20 μg ml^{-1}.[30] Chen *et al.* have shown a proof of concept of using GaN HEMTs for biomolecule detection at preliminary levels.[31] In our previous studies, we developed HEMTs for various sensing and biosensing applications such as heavy metal, pH, polar liquid, C-erbB2/HER2, and C3G detection.[32–37] The previously developed biosensor shows a reasonably good response for C-erbB2 (HER2) detection; however, it lacks robust surface biochemistry that limits the low-level detection of the targeted biomolecules. Also, it was demonstrated in human breast cancer cell lines that biopsy of the cell tissues from the affected area is required, making the testing invasive, challenging and less frequent. Here, we have improved the surface biochemistry by incorporating some intermediate steps (discussed in section 2.3) which allows for more efficient conjugation of the antibodies at physiological pH that leads to very low level (femtomolar) detection of the HER2 antigen. The reported biosensor has been successfully tested in a serum along with the Crk SH3-domain-binding guanine-nucleotide releasing factor (C3G) antigen as the control sample. The low level detection of HER2 in a serum makes this sensor useful for early-stage diagnosis with a non-invasive methodology. In this reported work, a GaN HEMT-based biosensor has been developed and tested on the antigen–antibody interaction principle for detecting HER2. The sensor has been tested for a broad range of concentration of HER2 from 0.7 pg ml^{-1} (5×10^{-15} M) to 10 μg ml^{-1} (6×10^{-8} M). The sensing performance has also been explored for long-term application and degradation. To immobilize the corresponding antibody on the sensor's gold sensing surface (gate area), thiol-based surface chemistry has been utilized. The sensor is characterized at each step of biofunctionalization to understand their impacts. Material and electrical characterization is carried out to observe the sensing area modification and *I–V* measurements. The developed GaN HEMT-based sensor has shown excellent performance and provides a robust point of care diagnostic tool for HER2 detection.

2 Materials and methods

2.1 Chemicals

Thioglycolic acid, also known as mercaptoacetic acid ($HSCH_2$-COOH), (98%; lab grade linker) was purchased from Sigma-Aldrich. Lab grade chemical reagents such as *N*-(3-dimethylaminopropyl)-*N*′-ethylcarbodiimide hydrochloride (EDC) ($C_8H_{17}N_3$·HCl) (98%), *N*-hydroxysuccinimide also known as 1-hydroxy-2,5-pyrrolidinedione ($C_4H_5NO_3$) (NHS) (98%) and sodium hydroxide (NaOH) were purchased from Sigma Aldrich. Buffer solutions, *i.e.*, phosphate buffered saline and 2-(*N*-morpholino)ethanesulfonic acid ($C_6H_{13}NO_4S$) for diluting the antigen and antibody, were procured from Sigma Aldrich as well. Bovine serum albumin (BSA) (98%) was procured from Sigma-Aldrich. A stock concentration of 100 μg ml^{-1} of the HER2 antibody [3B5] (product number ab16901) and recombinant human HER2 protein (Active) (product number ab60866) are obtained from Abcam, MA, USA and stored at −20 °C.

2.2 Fabrication of GaN HEMTs

Our previous studies have shown the fabrication of GaN HEMTs in detail. Fig. 1(a) summarises the most relevant steps during the fabrication process and shows an epitaxial structure of a fabricated HEMT along with the device design and epi-layer parameters. The molar fraction of aluminium

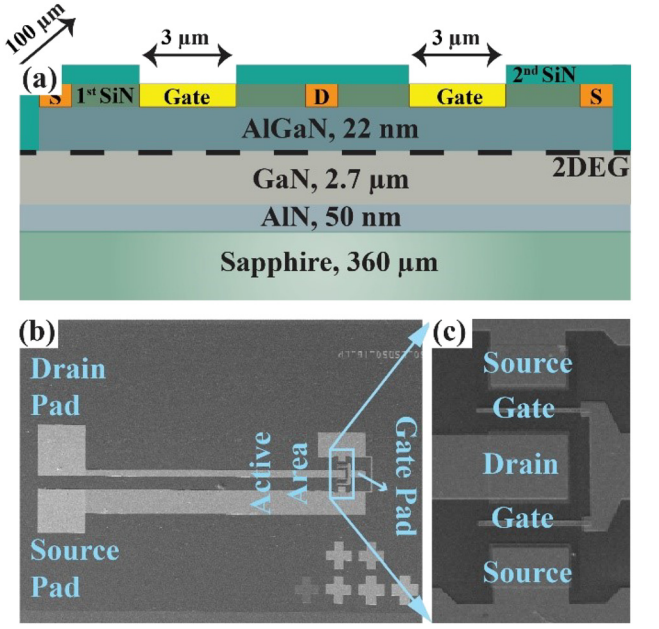

Fig. 1 GaN HEMT: (a) schematic illustration of the cross section view of the epitaxial and device design, (b) device with biasing pads and an active area, and (c) zoomed in view of the source, drain and gate, respectively.

in the AlGaN layer is 22%. The fabrication of the HEMT consists of 5 major process steps, *i.e.*, ohmic contacts, isolation, Schottky contacts, interconnection (biasing pads), and sensing area opening. To make ohmic contacts (source and drain), a metal stack of Ti/Al/Ni/Au with a thickness of 20/150/40/50 nm is deposited using an e-beam evaporation system followed by rapid thermal annealing at 830 °C for 30 s in a nitrogen environment that gives the ohmic contact resistance of 5×10^{-6} ohm per cm^2.[38] Interdevice isolation has been achieved using bombardment of nitrogen ions using an ion implantation method, which gives an isolation resistance of 10 GΩ. Schottky contacts (gate) have been deposited by a metal stack of Ni/Ti/Au with a thickness of 15/20/150 nm using an e-beam evaporation system. Finally, the entire surface of the devices has been coated with a Si_3N_4 layer with a thickness of 200 nm using the plasma enhanced chemical vapour deposition (PECVD) method, which is later selectively etched away from the sensing active area (gate) and biasing pads of the devices. Fig. 1(b and c) show the scanning electron microscopy images of the fabricated GaN HEMT with the labelling of an active area. Fig. 2 shows a graphical depiction of the process flow related to the fabrication of GaN HEMTs.

2.3 Antibody immobilization on the sensor

Functionalisation of a sensor aims to immobilise the antibody on the sensing area. However, the antibody receptors cannot be immobilised directly on the metal surface (sensing area). Functionalisation is a multistep process requiring a linker to bind the antibody receptors. In our case, thiol-based chemistry has been utilised to immobilise the HER2 antibodies on the gate area (sensing surface) of the GaN HEMTs. Thioglycolic acid (TGA) ($HSCH_2$-COOH) of 1 M concentration has been prepared by diluting 1 ml of concentrated TGA in 9.3 ml of deionised (DI) water. The GaN HEMTs have been incubated in the TGA solution for 15 hours at room temperature. Later, the devices are rinsed three times with DI water. The thiol group (R–SH) in the TGA is attached to the gold surface (active/gate region) that makes a gold–sulfur (Au–S) complex, and the carboxylic group (R–COOH) is accessible at another end.[39,40] To confirm

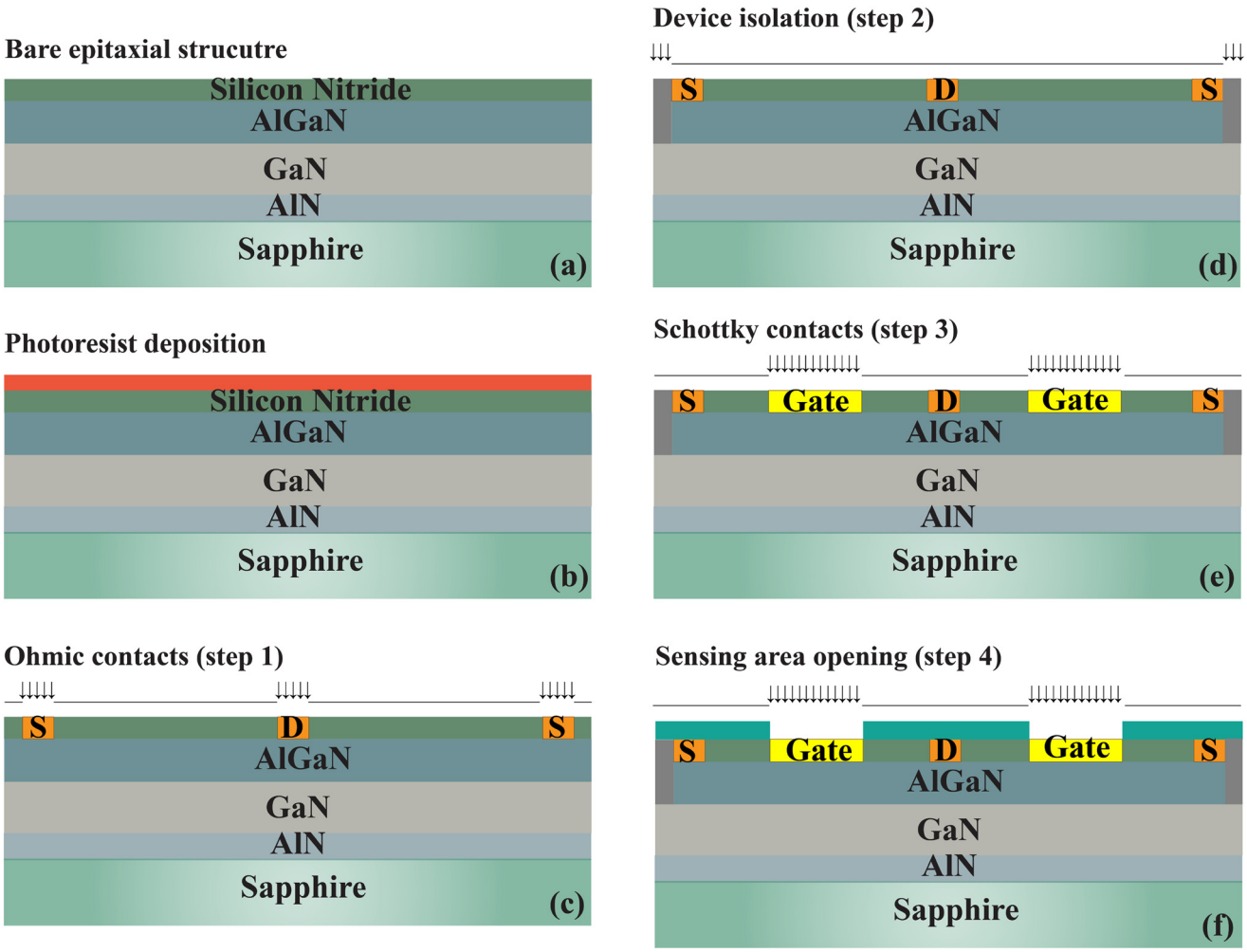

Fig. 2 Graphical illustration of the fabrication flowchart of GaN HEMTs. (a) Bare epitaxial structure, (b) photoresist deposition, (c) ohmic contacts formation, (d) device isolation, (e) Schottky contacts formation, (f) sensing area opening.

the formation of the TGA layer on the surface, Raman spectroscopy and Fourier transform infrared spectroscopy (FTIR) have been performed along with the electrical measurement of the sensor.

To improve the robustness of the surface biochemistry, EDCNHS coupling has been incorporated as an intermediate step. EDC converts free carboxylic groups (R–COOH) to prime amines typically *via* the formation of amine-reactive NHS-esters that are considerably more stable than amine-reactive intermediates and provides higher coupling efficiency for conjugation of the antibodies at physiological pH.[41–43] This coupling is accomplished by mixing EDC with an acid-containing molecule and adding NHS. In our case, a solution of EDC and NHS of 1 molar (M) concentration has been prepared in DI water and to provide an acidic environment, MES buffer with 6.1 pH has been mixed to prepare the final EDC/NHS solution. The devices are incubated in the prepared EDC/NHS solution for 2 hours at room temperature. The EDC/NHS surface chemistry forms a stable amine reactive site suitable for antibody binding. To bind the HER2 antibody, the devices are incubated in the diluted HER2 antibody in MES with a ratio of 1 : 1000 for 1 hour at room temperature. The immobilisation of the antibody receptors has been confirmed with a popular method in bioengineering known as enzyme-linked immunosorbent assay (ELISA). Finally, a blocking layer is formed on the surface that enhances the reaction between the antigen and antibody and blocks the unspecific sites that provide higher specificity for the HER2 antigen. BSA has been used at 2% concentration in DI water, and the devices are incubated for 2 hours at room temperature. In each process, the devices are rotated at 150 RPM for uniform coating of the corresponding layers. The *I–V* measurement of the devices has been carried out before and after each functionalisation step. Fig. 3 shows a graphical illustration of the functionalisation process along with the surface chemistry (stick diagrams) on the sensing areas (gold strips).

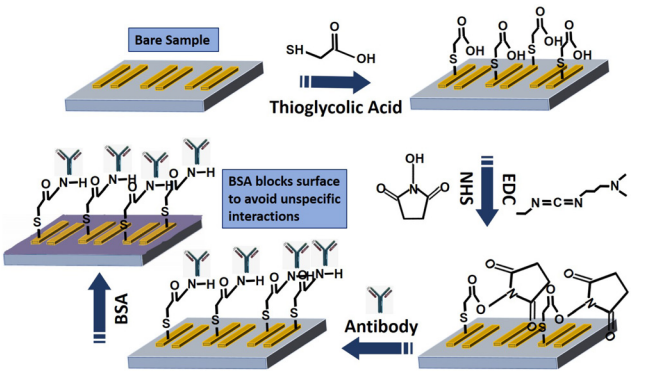

Fig. 3 Graphical illustration of the functionalisation process along with the chemical stick diagram on the surface. The direction of the arrows shows the process flow. Parallel yellow strips represent the gate of the HEMT (not drawn to scale).

3 Results and discussion

3.1 GaN HEMT DC characterization

The electrical characterization of the GaN HEMT has been carried out in a dry environment by measuring the DC output and transfer characteristics as a function of drain and gate voltages, as shown in Fig. 4. Output family curves of drain current–drain voltage (I_{ds}–V_{ds}) are shown in Fig. 4 (left) at different gate voltages from −3 V to 1.0 V with a 1.0 V step size. Fig. 4 (right) shows the DC transfer characteristics between the drain current and gate voltage (I_{ds}–V_{gs}) at a V_{ds} of +10 V. The maximum drain current obtained from the I_{ds}–V_{ds} curves is 53 mA at V_{gs} = +1 V and the maximum transconductance ($G_{m,max}$) and threshold voltage (V_{th}) obtained from the I_{ds}–V_{gs} curves are 15.4 mS and −2.8 V, respectively. *I–V* characteristics of the fabricated GaN HEMT show a well-known transistor action.

3.2 Immobilization of the HER2 antibody

The immobilization process of the HER2 antibody on the sensing area of the GaN HEMT begins with the thiol modification of the surface. Fig. 5(a) shows the Raman spectra of the sensing area before (black) and after (red) the incubation of the sensor in 1 M concentration of thioglycolic acid. The sample has been scanned from a wavelength of 150 to 2000 cm^{-1} using a 785 nm laser source. Sulphur (thiol group) present in TGA has a great affinity to bind with the gold surface and consequently forms an Au–S complex in the sensing area. The Au–S bond has been confirmed by a peak at around the wavelength of 260 cm^{-1}. The observed peak is well reported in the literature that confirms the suitable incubation of the sensor.[44–46]

Fourier transform infrared (FTIR) spectroscopy has been further performed to confirm the thiol functionalization. FTIR on the sensing surface after thiol modification has been carried out using FTIR equipment (BRUKER Tensor 37) from a wavelength of 2000 to 3500 cm^{-1}. IR spectra of TGA have also been obtained for reference and shows the stretching frequencies of S–H, C–H and O–H bonds. Thiol molecules bound to the gold surface through the Au–S bond have been confirmed by revealing the presence of S–H groups located at the band of 2565 cm^{-1} for TGA (Fig. 5(b-1)) and their disappearance at the same band on the Au surface (Fig. 5(b-2)), respectively. The most important distinction between the two FTIR spectra could be clearly determined by the band at

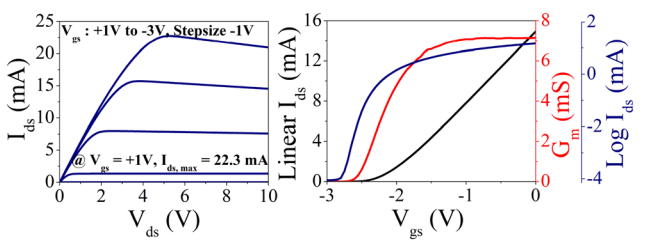

Fig. 4 Three terminal DC characterization of the fabricated GaN HEMT. Output characteristics (left) and transfer characteristics (right).

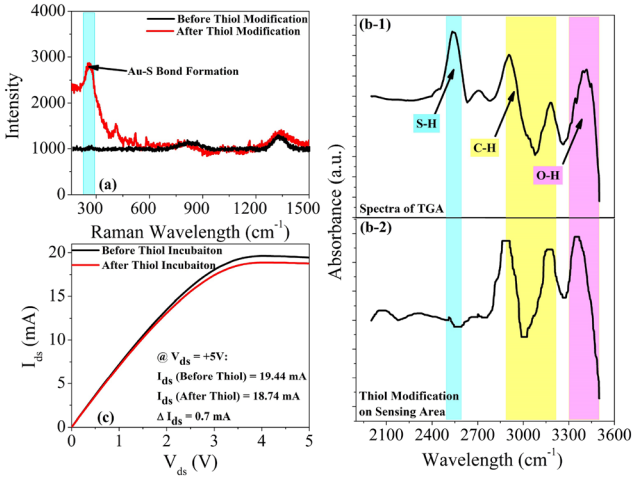

Fig. 5 (a) Raman spectroscopy of the sensing area before (black) and after (red) thiol modification. The Au–S peak is obtained at a wavelength of 265 cm^{-1}. (b) FTIR spectra (absorbance) of the sensing area (b-1) before and (b-2) after thiol modification. Disappearance of the S–H bond in (b-2) proves the formation of the Au–S complex. (c) Drain current measurement of the sensor before (black) and after (red) thiol incubation.

2565 cm^{-1} assigned to S–H bonding on the top spectrum. However, this band is not present in the bottom spectrum. This can be attributed to the cleavage of the S–H bond that led to the formation of a new bond, *i.e.*, the Au–S bond.[47,48] This phenomenon proved the fact that thiol-terminated TGA is bound onto the gold surface. Other peaks related to a carboxylic group, such as C–H and O–H, are found at a wavelength of 2920 and 3350 cm^{-1}, respectively.[49,50] These facts further proved that the TGA molecules are bound to the Au surface through the Au–S bond at one end while the functional carboxyl groups (–COOH) freely moved to the other end. These remarks are in good agreement with those reported by Aryal *et al.* and Królikowska *et al.*, who have covered the formation of the COOH-terminated TGA bound to the gold surface through new Au–S bonding related to the absence of thiol (S–H) molecules.[47,51]

The impact of thiol modification on the sensing area has also been studied electrically by taking the *I–V* measurements of the sensor before and after thiol incubation. Fig. 5(c) shows the *I–V* measurement of the sensor as a function of drain to source voltage. The drain current of the sensor increases after the thiol modification confirms the abundance of positive charges on the gate terminal. A biochemical process on the surface of the gate alters the charge composition on the gate surface, which is reflected by the change in the drain current that proves the surface modification due to a specific biochemical process.

To immobilize the antibody receptors on the sensing area, the activated carboxylic group has been incubated in the HER2 antibody. The immobilization of HER2 antibody receptors has been confirmed through the ELISA method. For reference, the method can be summarized as follows. The HER2 antibody receptors are immobilized using the aforementioned functionalization process, and the targeted HER2 antigen is conjugated on the antibody receptors. Later, a corresponding secondary antibody linked with a specific colour-producing enzyme has been used, which binds with the HER2 antigen. Finally, a substrate is added to the samples. ELISA is usually chromogenic using a reaction that converts the substrate (*e.g.*, 3,3′,5,5′-tetramethylbenzidine) into a coloured product which can be measured using an optical density spectrometer. The process of performing ELISA on the GaN HEMTs is graphically illustrated in Fig. 6(a). Optical images of the diced GaN HEMT sensors after secondary antibody (AB) and after 3,3′,5,5′-tetramethylbenzidine (TMB) assays (coloration) along with the optical density (OD) are shown in Fig. 6(b). It can be seen that the obtained optical density for the sensors is greater than 0.6, which generally indicates the formation of the antibody and antigen conjugate.[52] If the primary antibody is not immobilized on the surface, the TMB will not produce any colour; however, in our case, the ODs are reasonably good, which indicates a suitable immobilization of the antibody receptors.

Apart from ELISA, the antibody immobilization on the sensing area (gate) has been confirmed by *I–V* characterization of the biosensor as shown in Fig. 6(c). The drain current has been measured before and after the antibody incubation as a function of the drain to source voltage. The drain current increases after the antibody immobilization, which also strengthens the confirmation of suitable immobilization of antibody receptors. As per the functionalization process, the sensors are incubated in 2% BSA solution (2 mg ml^{-1}) to block the unexpected remaining unspecific sites on the sensing area to avoid cross interaction

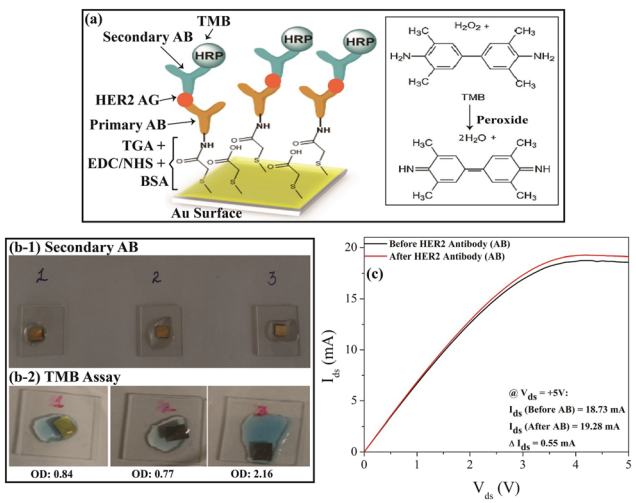

Fig. 6 (a) Graphical depiction of the ELISA process on the fabricated diced GaN HEMTs along with the labelling (not drawn to scale). (b) Optical images of the diced GaN HEMT sensors (b-1) after the secondary antibody and (b-2) after TMB assays. An optical density greater than 0.6 confirms suitable immobilization of the HER2 antibody receptor on the sensing area. (c) *I–V* measurement of the sensor before (black) and after (red) the HER2 antibody incubation.

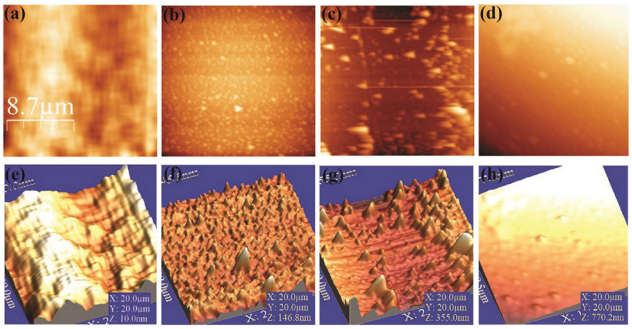

Fig. 7 Images of the sensor in 2D (first row) and 3D (second row) obtained using atomic force microscopy at various functionalization steps. (a and e) Bare gold, (b and f) after thiol incubation, (c and g) after antibody immobilization and (d and h) after BSA incubation. Roughness of the surface has been also mentioned in the respective 3D images.

of nonspecific species present in the test solution. Moreover, the study of the surface modification of the sensing area after each biochemical process has also been observed using atomic force microscopy (AFM), as shown in Fig. 7. The roughness and morphology of the surface after each process also prove the surface modification at the physical level. The surface roughness of the bare device is around 10 nm, increasing to 146.8, 355 and 770.2 nm after its modification in thiol, antibody and BSA, respectively. All these presented results prove the suitable immobilization of antibody receptors on the sensing area of the GaN HEMT.

3.3 Detection of the HER2 antigen

After the successful immobilization of the HER2 antibody, the biosensor can be used for testing the HER2 antigen. Fig. 8 shows the response of the sensor for two different concentrations of the HER2 antigen (AG), *i.e.*, 0.1 and 1 μM as a function of the drain to source voltage (navy and olive lines, respectively) along with the complete functionalization process steps. A drop-cast method has been used on the sensing area of the sensor, which requires only 3 μl volume of the test antigen. The drain current increases after the HER2 antigen incubation. As BSA incubation is the final step of the functionalization process, the drain current (magenta) after the BSA incubation has been taken as the reference for relative measurements and conclusions. A control sample has also been used to test the device's specificity. It can be noted that the change in the drain current after dropping the control sample (purple) is negligible as compared to the targeted antigen.

In the colour-based immunoassay, it is well recognized that BSA improves the specificity of a sensor. However, in the solid state-based immunoassay, the BSA's role is unclear. To understand this aspect, testing of the HER2 antigen is carried out on two different sensors where one is incubated with BSA, and another is used without incubation. Three different concentrations of the HER2 antigen *i.e.*, 100 ng ml^{-1}, 1 μg ml^{-1} and 10 μg ml^{-1}, have been tested. Fig. 9 shows the sensor's response at a V_{ds} of +5 V, and it can be clearly observed that for any concentration, the response of the sensor incubated in BSA is better. Exposing the sensing area to BSA after coating causes the free binding sites on the sensing area to become saturated. This minimizes the possibility of non-specific binding and significantly improves the signal-to-noise ratio. This study clearly demonstrates that the BSA incubation improves the specificity and the sensitivity of the sensor.

The incubation time of the antigen means the time required for the antigen to form a suitable antigen–antibody

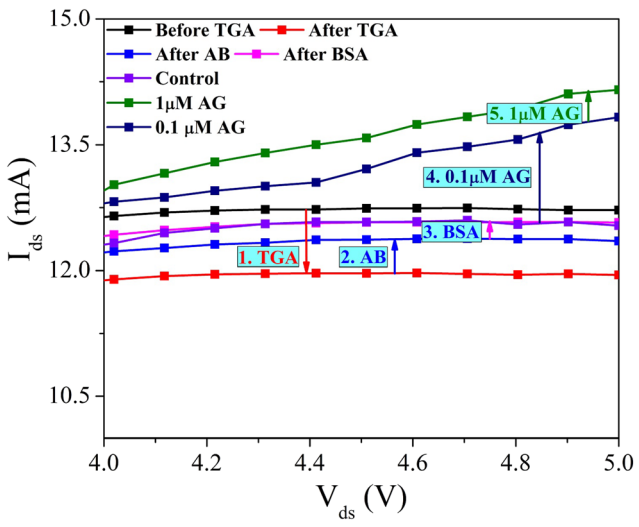

Fig. 8 Drain current measurement of the biosensor as a function of interactions among TGA, HER2-antibody, BSA, control sample, and HER2 antigen (0.1 and 1 μg ml^{-1}). The direction of arrows represents the moment of the drain current after a particular process.

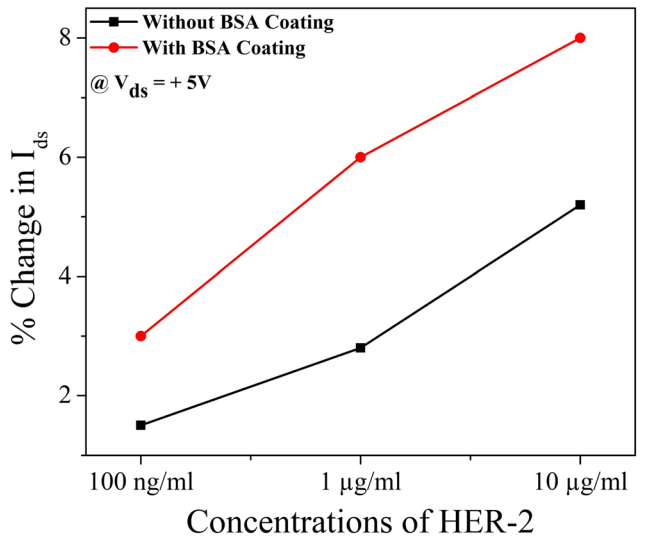

Fig. 9 Percentage change in the drain current for various concentrations of the HER2 antigen for the BSA coated (block nonspecific interactions) (red) and without BSA (no blocking) (black) sensors.

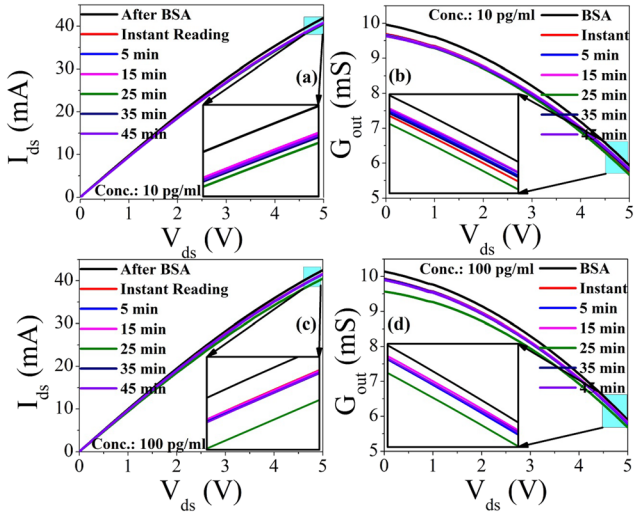

Fig. 10 Response of the sensor for various incubation times of the antigen at two different concentrations of 10 and 100 pg ml^{-1}. (a and c) The drain current variation and (b and d) the channel conductance of the sensor. The optimum response of the sensor is obtained for the incubation of 25 min.

complex by their interaction with the sensing area. The impact of the incubation time on the drain current has been systematically studied. Two different concentrations of the HER2 antigen, *i.e.*, 10 and 100 pg ml^{-1}, have been prepared, and multiple experiments have been performed where the incubation time of the sensors has been varied. The drain current has been measured after each incubation. Fig. 10(a and c) show the drain current of the sensor for various incubation times from instant reading to 45 min for 10 and 100 pg ml^{-1} concentrations of HER2, respectively. The output conductance of the sensor has also been measured as a function of V_{ds} and incubation time as shown in Fig. 10(b and d). It can be seen from Fig. 10 that for both the concentrations, the highest change in the drain current and the output conductance is obtained for an incubation time of 25 min. Insets in Fig. 10 show the zoomed in view of the drain current and the output conductance for both the concentrations at V_{ds} from 4.5 to 5 V. Percentage change in the drain current at the V_{ds} of +5 V *vs.* incubation time has also been plotted and is shown in Fig. 11 demonstrating that the optimum incubation time for the antigen–antibody interaction is around 25 min. Prolonged incubation (>0.5 hours) of the sensors in the HER2 antigen test solution can cause the antigen–antibody complexes to dissociate at room temperature.[53,54] The antigen–antibody complex/activity degradation and washing of the samples reduce the net charge on the sensing area (gate) for the same concentration. This charge reduction leads to a smaller change in the drain current for an incubation time of more than half an hour.

Another set of experiments has been carried out to assess the long-term performance of the biosensor. In this experiment, the HER2 antigen is drop-casted on the sensing area, and the reading of the drain current has been recorded after a specific time, as shown in Fig. 12. The drain current after BSA incubation (before HER2 antigen incubation) is taken as the reference. Fig. 12(a) shows that the drain current increases at 25 min (blue) and begins to decrease after 18 hours (magenta). The same sample is measured after three days which exhibited a further reduction in the drain current (green), and the drain current approximately reaches the value of before antigen case (after BSA (black)). Fig. 12(b) presents the summarized form of the experiment where absolute (black) and relative (red) changes in the drain current with respect to the BSA level are shown for various measurement times at a V_{ds} of +5 V. Furthermore, the stability of the biosensor is tested over 200 hours at room temperature. Throughout the time period, the biosensor shows a ±2% change in the drain current.

The biosensor has been tested to detect the HER2 antigen in a serum in its clinically relevant concentration range from 1 to 50 ng ml^{-1}. At the same time, the specificity study of the biosensor has also been explored in more detail. The Crk SH3-domain-binding guanine-nucleotide-releasing factor

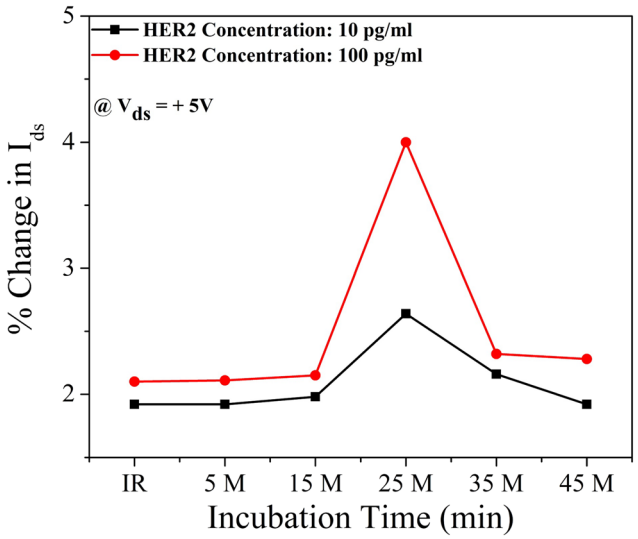

Fig. 11 Percentage change in the drain current as a function of the incubation time at two concentrations *i.e.*, 10 pg ml^{-1} (black) and 100 pg ml^{-1} (red) of the antigen at a V_{ds} of +5 V.

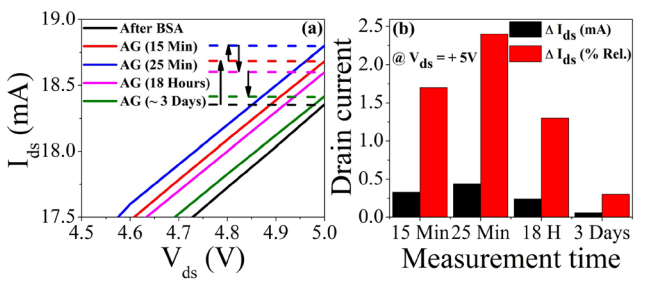

Fig. 12 Long-time testing of the sensor. (a) Drain current measurement of the sensor at various time intervals. (b) Absolute change (black) and relative change (red) in the drain current at a V_{ds} of +5 V.

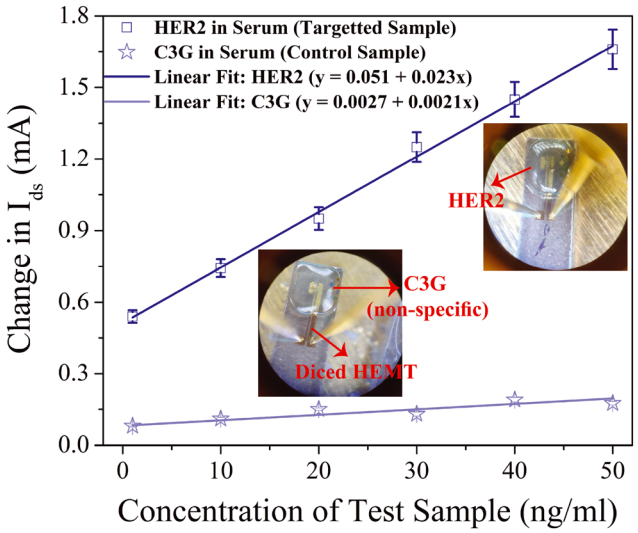

Fig. 13 Response of the biosensor for various concentrations of the HER2 antigen in a serum. The C3G antigen is the non-specific antigen (control samples) in the same concentration range.

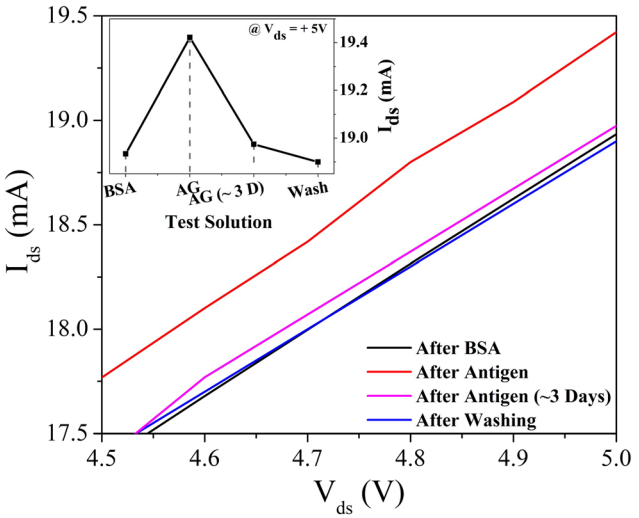

Fig. 15 Drain current response of the sensor after BSA and antigen incubation and washing. After washing, the drain current returns to its reference (BSA) value. The inset presents the drain current after washing at a V_{ds} of +5 V.

(C3G) antigen is used as the non-specific antigen (control samples) in the same concentration range as the HER2 (1 to 50 ng ml^{-1}). The C3G antigen is found in the human body, regulates cell proliferation, and helps cell adhesion. C3G also plays a crucial role in regulating Ras family GTPases, leading to mitogen-activated protein kinase activation. Ideally, the biosensor should show a negligible response to C3G (control samples) compared to HER2 (targeted samples). Fig. 13 shows the response of the biosensor for the HER2 and C3G antigens at a drain to source voltage (V_{ds}) of +5 V. The biosensor's response to the HER2 antigen has excellent linear characteristics and is significantly higher than that to the C3G antigen. Even for a 50 times larger concentration of C3G (50 ng ml^{-1}), the sensor's response is almost negligible compared to the HER2 antigen (1 ng ml^{-1}). The biosensor's response to HER2 can be easily distinguished from the non-specific antigens and control samples, showing the developed biosensor's high specificity.

One of the advantages of using a solid-state-based biosensor is its reusability. To explore this important aspect, the sensing area of the biosensor has been rinsed with the PBS buffer solution first and later washed through the standard semiconductor cleaning process. Imaging the surface of the biosensor using scanning electron microscopy (SEM) and *I–V* measurement has been performed to assess the reusability. Fig. 14 shows the SEM images before (Fig. 14(a)) and after (Fig. 14(a)) the cleaning process. It can be clearly seen that those patches of the HER2 antigen on the surface before cleaning are completely removed after washing. The *I–V* measurement shown in Fig. 15 also proves that the antigen–antibody complex has been removed after

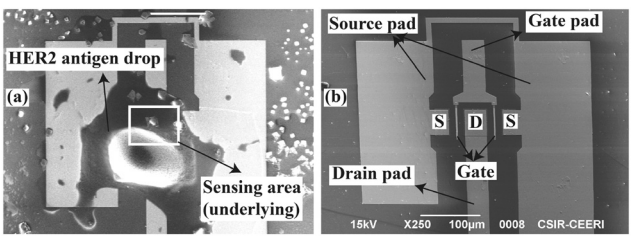

Fig. 14 Images of the sensor obtained using a scanning electron microscope. The HER2 antibody–antigen complex (a) before and (b) after washing of the surface along with labels.

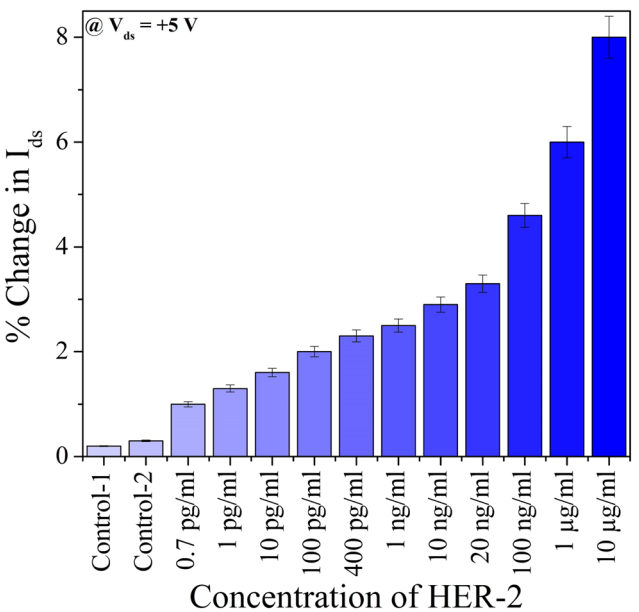

Fig. 16 Percentage change in the drain current for a broad range of concentration of the HER2 antigen from 0.7 pg ml^{-1} to 10 μg ml^{-1} at a V_{ds} of +5 V. Control samples show negligible current change as compared to the HER2 antigen.

washing, and the drain current returns to its reference value. An inset is provided in Fig. 15 that shows the drain current at the V_{ds} of +5 V and compares its value at various measurement steps. Return of the drain current to its reference value and the surface imaging captured by SEM confirm that the biosensor platform is reusable.

Finally, the biosensor has been tested for a broad dynamic range of the concentration of the HER2 antigen. Fig. 16 presents the performance of the biosensor as a change in the drain current for the HER2 antigen concentration from 0.7 pg ml^{-1} to 10 μg ml^{-1} at a V_{ds} of +5 V. Two control samples have also been tested to validate the specificity of the biosensor. The response to the control samples is negligible compared to that to the HER2 antigen. The voltage sensitivity of the biosensor for HER2 detection has been calculated using the same methodology reported in our previous work,[37] and it is estimated to be a 124 mV per decade concentration of HER2. Additionally, the three-sigma method has been used to extract the biosensor's limit of detection (LOD).[55] The proposed AlGaN/GaN-based biosensor has an LOD of 0.58 pg ml^{-1} (4.21 fM) for HER2 detection. The developed sensor can clearly detect as low as pg ml^{-1} range of concentrations of the HER2 antigen. A brief comparison of our work and previously reported studies is summarized in Table 1.

Fig. 17 summarizes the result shown in Fig. 16 based on the Langmuir isotherm that focuses on the equilibrium surface coverage of the antibody as a function of the analyte concentrations.[56,57] The analysis establishes a relationship between the source to drain current (I_{ds}) and the surface coverage of the antibody receptors. Here, the three-binding-site model has been used to fit the curve properly, and the antigen–antibody chemical reactions are described below:

$$\begin{aligned}[Ab]_{site1} + [Ag] \langle = \rangle [Ag-Ag]_{site1} * K_{D1} \\ [Ab]_{site2} + [Ag] \langle = \rangle [Ag-Ag]_{site2} * K_{D2} \\ [Ab]_{site3} + [Ag] \langle = \rangle [Ag-Ag]_{site3} * K_{D3}\end{aligned} \quad (1)$$

where K_{D1}, K_{D2} and K_{D3} are the dissociation constants for the binding sites on an antibody receptor. The total current change is assumed to be the sum of the current change resulting from the antibody–antigen complex at three sites, as given in eqn (2):

$$\Delta I_{ds} = \Delta I_{ds1} + \Delta I_{ds2} + \Delta I_{ds3} \quad (2)$$

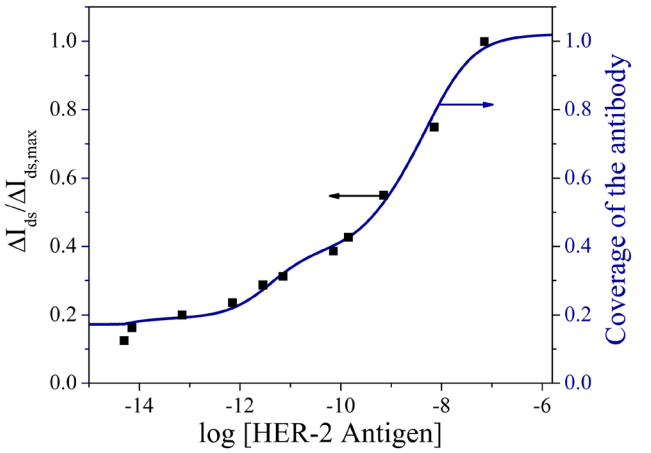

Fig. 17 Antibody surface coverage ratio (blue) as a function of the HER2 antigen concentration. The $\Delta I_{ds}/\Delta I_{ds,max}$ ratio (black solid squares) obtained from the experimental results *versus* the antigen concentration is shown as well.

For the single site model, the surface coverage ratio (θ) can be obtained in eqn (3) in terms of the drain current and dissociation constant:

$$\theta = \frac{\Delta I_{ds}}{\Delta I_{ds,max}} = \frac{1}{1 + K_D/[Ag]} = \frac{[Ab-Ag]}{[Ab]_{max}} \quad (3)$$

where the total antibody concentration $[Ab]_{max}$ is the sum of the unbound antibody concentration and the antibody–antigen complex concentration ([Ab − Ag]). For our model, change in the drain current (ΔI_{ds}) can be given as eqn (4) by following eqn (3):

$$\Delta I_{ds} = \frac{\Delta I_{ds1,max}}{1 + K_{D1}/[Ag]} + \frac{\Delta I_{ds2,max}}{1 + K_{D2}/[Ag]} + \frac{\Delta I_{ds2,max}}{1 + K_{D3}/[Ag]} \quad (4)$$

The binding sites at an antibody are almost identical, and thus, it is reasonable to assume equal current contributions from each side that provide an equal contribution to the current change at the output. Eqn (4) is fitted into the experimental results, providing the values of K_{D1}, K_{D2} and K_{D3} being 7 × 10^{-10} M, 8.8 × 10^{-11} M, and 7.2 × 10^{-9} M, respectively. The obtained dissociation constants are in a reasonable range of regular antibody–antigen binding dissociation constants.[58–60] According to the values of the dissociation constants and eqn (3), the surface coverage ratio of the antibody receptors *vs.* the concentration of the HER2 antigen is plotted in Fig. 17 exhibiting the expected S-shaped curve (blue).

Table 1 A comparison of the previously reported work and our work based on the amplification technique, sensing platform, dynamic range and LOD

Ref.	Signal amplification	Detection method	Dynamic range	LOD
Joshi *et al.*[61]	DSN/ARANPs	SERS	12 fM to 18 pM	5 fM
Myung *et al.*[62]	APTES	Graphene-based FET	12 fM to 1 μM	1 pM
Chen *et al.*[31]	Antibody–antigen	GaN HEMTs	0.25 to 16.7 μg ml^{-1}	0.25 μg ml^{-1}
Our Work	Antibody–antigen	GaN HEMTs	5 fM to 60 nM	4.21 fM

4 Conclusions

The AlGaN/GaN HEMT-based biosensor demonstrates a great potential for the quantitative measurements of the HER2 antigen with morphological confirmation of the HER2 antibody immobilization. The developed sensor has shown the detection of the HER2 antigen in the range of 0.7 pg ml^{-1} to 10 μg ml^{-1}. The sensor offers a good specificity toward the HER2 antigen, which is demonstrated using control samples. The thiol-based chemistry has been utilized to immobilize the antibody on the sensing surface. Confirmation of the thiol functionalization has been performed by Raman and FTIR analysis along with the morphological study using AFM. The immobilization of the antibody receptors has been verified using the ELISA of the sensing area and *I–V* measurements of the biosensor. The impact of the BSA blocking has also been studied, along with the optimization of the antibody and antigen incubation time to obtain a maximum response. A long time study of the sensor after antigen incubation has also been performed to understand the practicability of the sensor. The developed sensor can be reused after washing the sensing area. The three-binding-site model based on the Langmuir isotherm has also been developed with the three dissociation constants extracted from the analysis of the experimental results. The developed biosensor has a promising future in the *in vitro* diagnostics industry, particularly homecare diagnostics, owing to the short response time and low sample requirement (2.5–5) μl with high specificity towards a targeted analyte.

Conflicts of interest

There are no conflicts to declare.

Acknowledgements

The authors gratefully acknowledge the support from the CSIR – Nano Biosensor and Microfluidics Mission Mode project, budget head – HCP0012. The authors are also thankful to the director of CSIRCEERI, Pilani.

Notes and references

1 N. Iqbal and N. Iqbal, Human Epidermal Growth Factor Receptor 2 (HER2) in Cancers: Overexpression and Therapeutic Implications, *Mol. Biol. Int.*, 2014, **2014**, 1–9, DOI: **10.1155/2014/852748**.

2 M. M. Moasser, The oncogene HER2: Its signaling and transforming functions and its role in human cancer pathogenesis, *Oncogene*, 2007, **26**(45), 6469–6487, DOI: **10.1038/sj.onc.1210477**.

3 W. Tai, R. Mahato and K. Cheng, The role of HER2 in cancer therapy and targeted drug delivery, *J. Controlled Release*, 2010, **146**(3), 264–275, DOI: **10.1016/j.jconrel.2010.04.009**.

4 A. Perrier, J. Gligorov, G. Lefevre and M. Boissan, The extracellular domain of Her2 in serum as a biomarker of breast cancer, *Lab. Invest.*, 2018, **98**(6), 696–707, DOI: **10.1038/s41374-018-0033-8**.

5 B. Leyland-Jones, *et al.*, Utility of serum HER2 extracellular domain assessment in clinical decision making: Pooled analysis of four trials of trastuzumab in metastatic breast cancer, *J. Clin. Oncol.*, 2009, **27**(10), 1685–1693, DOI: **10.1200/JCO.2008.16.8351**.

6 S. Ahn, J. W. Woo, K. Lee and S. Y. Park, HER2 status in breast cancer: Changes in guidelines and complicating factors for interpretation, *J. Pathol. Transl. Med.*, 2020, **54**(1), 34–44, DOI: **10.4132/jptm.2019.11.03**.

7 J. Zhao and Y. Xia, Targeting HER2 Alterations in Non–Small-Cell Lung Cancer: A Comprehensive Review, *JCO Precis. Oncol.*, 2020(4), 411–425, DOI: **10.1200/po.19.00333**.

8 K. Egebjerg, C. D. Harwood, N. C. Woller, C. A. Kristensen and M. Mau-Sorensen, HER2 Positivity in Histological Subtypes of Salivary Gland Carcinoma: A Systematic Review and Meta-Analysis, *Front. Oncol.*, 2021, **11**(June), 1–12, DOI: **10.3389/fonc.2021.693394**.

9 F. A. M. Lucas and S. N. Cristovam, HER2 testing in gastric cancer: An update, *World J. Gastroenterol.*, 2016, **22**(19), 4619–4625, DOI: **10.3748/wjg.v22.i19.4619**.

10 K. Egebjerg, R. S. Garbyal, J. P. Hasselby, L. Baeksgaard and M. Mau-Sorensen, Prevalence of HER2 overexpression and amplification in squamous cell carcinoma of the esophagus: A systematic review and meta-analysis, *Crit. Rev. Oncol. Hematol.*, 2021, **161**, 103339, DOI: **10.1016/j.critrevonc.2021.103339**.

11 Y. W. Chung, *et al.*, Overexpression of HER2/HER3 and clinical feature of ovarian cancer, *J. Gynecol. Oncol.*, 2019, **30**(5), 1–12, DOI: **10.3802/jgo.2019.30.e75**.

12 B. Shekhar, *et al.*, Evaluation of prevalence and prognostic significance of human epidermal growth factor receptor 2/neu expression in carcinoma endometrium, *Int. J. Mol. Immuno Oncol.*, 2020, **5**(1), 8–13, DOI: **10.25259/i jmio202019**.

13 S. Tian, K. Zeng, A. Yang, Q. Wang and M. Yang, A copper based enzyme-free fluorescence ELISA for HER2 detection, *J. Immunol. Methods*, 2017, **451**(August), 78–82, DOI: **10.1016/j.jim.2017.09.002**.

14 W. R. Chao, *et al.*, Assessment of HER2 status using immunohistochemistry (IHC) and fluorescence in situ hybridization (FISH) techniques in mucinous epithelial ovarian cancer: A comprehensive comparison between ToGA biopsy method and ToGA surgical specimen method, *PLoS One*, 2015, **10**(11), 1–10, DOI: **10.1371/journal.pone.0142135**.

15 S. Agersborg, *et al.*, Immunohistochemistry and alternative FISH testing in breast cancer with HER2 equivocal amplification, *Breast Cancer Res. Treat.*, 2018, **170**(2), 321–328, DOI: **10.1007/s10549-018-4755-5**.

16 S. Sakamoto, *et al.*, Enzyme-linked immunosorbent assay for the quantitative/qualitative analysis of plant secondary metabolites, *J. Nat. Med.*, 2018, **72**(1), 32–42, DOI: **10.1007/s11418-017-1144-z**.

17 S. W. Kim, J. Roh and C. S. Park, Immunohistochemistry for pathologists: Protocols, pitfalls, and tips, *J. Pathol. Transl. Med.*, 2016, **50**(6), 411–418, DOI: **10.4132/jptm.2016.08.08**.

18 D. Huber, L. V. von Voithenberg and G. V. Kaigala, Fluorescence in situ hybridization (FISH): History, limitations and what to expect from micro-scale FISH?, *Micro Nano Eng.*, 2018, **1**, 15–24, DOI: **10.1016/j.mne.2018.10.006**.

19 M. Kaisti, Detection principles of biological and chemical FET sensors, *Biosens. Bioelectron.*, 2017, **98**(April), 437–448, DOI: **10.1016/j.bios.2017.07.010**.

20 K. T. Upadhyay and M. K. Chattopadhyay, Sensor applications based on AlGaN/GaN heterostructures, *Mater. Sci. Eng. B: Solid-State Mater. Adv. Technol.*, 2021, **263**(September), 114849, DOI: **10.1016/j.mseb.2020.114849**.

21 R. Kirste, N. Rohrbaugh, I. Bryan, Z. Bryan, R. Collazo and A. Ivanisevic, Electronic Biosensors Based on III-Nitride Semiconductors, *Annu. Rev. Anal. Chem.*, 2015, **8**, 149–169, DOI: **10.1146/annurev-anchem-071114-040247**, Epub 2015 May 27, PMID: 26048553.

22 R. Vetury, Polarization Induced 2DEG in Al–GaN/GaN HEMTs: On the origin, DC and transient characterization, *PhD thesis*, University of California, Santa Barbara, 2000.

23 L. Gu, S. Yang, B. Miao, Z. Gu, J. Wang and W. Sun, Electrical detection of trace zinc ions with an extended gate-AlGaN/GaN high electron mobility sensor, *Analyst*, 2019, **144**(2), 663–668, DOI: **10.1039/c8an01770k**.

24 Y. Dong, *et al.*, AlGaN/GaN heterostructure pH sensor with multi-sensing segments, *Sens. Actuators, B*, 2018, **260**, 134–139, DOI: **10.1016/j.snb.2017.12.188**.

25 B. H. Chu, *et al.*, Wireless detection system for glucose and pH sensing in exhaled breath condensate using A1GaN/GaN high electron mobility transistors, *IEEE Sens. J.*, 2010, **10**(1), 64–70, DOI: **10.1109/JSEN.2009.2035213**.

26 B. S. Kang, *et al.*, Prostate specific antigen detection using AlGaNGaN high electron mobility transistors, *Appl. Phys. Lett.*, 2007, **91**(11), 2005–2008, DOI: **10.1063/1.2772192**.

27 H. T. Wang, *et al.*, Electrical detection of kidney injury molecule-1 with [formula omitted] high electron mobility transistors, *Appl. Phys. Lett.*, 2007, **91**(22), 1448, DOI: **10.1063/1.2815931**.

28 I. Sarangadharan, *et al.*, High sensitivity cardiac troponin I detection in physiological environment using Al–GaN/GaN High Electron Mobility Transistor (HEMT) Biosensors, *Biosens. Bioelectron.*, 2018, **100**(September), 282–289, DOI: **10.1016/j.bios.2017.09.018**.

29 H. H. Lee, *et al.*, AlGaN/GaN high electron mobility transistorbased biosensor for the detection of C-reactive protein, *Sensors*, 2015, **15**(8), 18416–18426, DOI: **10.3390/s150818416**.

30 F. Ren, B. H. Chu, K. H. Chen, C. Y. Chang, V. Chen and S. J. Pearton, GaN-Based Sensors, in *GaN and ZnO-based Materials and Devices, Springer Series in Materials Science*, ed. S. Pearton, Springer, Berlin, Heidelberg, 2012, vol. 156, DOI: **10.1007/978-3-642-23521-4_6**.

31 K. H. Chen, *et al.*, C-erbB-2 sensing using AlGaNGaN high electron mobility transistors for breast cancer detection, *Appl. Phys. Lett.*, 2008, **92**(19), 2006–2009, DOI: **10.1063/1.2926656**.

32 S. Mishra, P. Kachhawa, R. R. Thakur, A. K. Jain, K. Singh and N. Chaturvedi, Detection of heavy metal ions using meander gated GaN HEMT sensor, *Sens. Actuators, A*, 2021, **332**, 113119, DOI: **10.1016/J.SNA.2021.113119**.

33 N. Chaturvedi, *et al.*, AlGaN/GaN HEMT based sensor and system for polar liquid detection, *Sens. Actuators, A*, 2020, **302**, 111799, DOI: **10.1016/j.sna.2019.111799**.

34 N. Chaturvedi, R. Chowdhury, S. Mishra, K. Singh, N. Chaturvedi, A. Chauhan, S. Pande, N. Sharma, P. Parjapat, R. Sharma, P. Kothari and A. K. Singh, GaN HEMT based biosensor for the detection of breast cancer marker (C-erbB2), *Semicond. Sci. Technol.*, 2021, **36**(4), 045018, DOI: **10.1088/1361-6641/abe83e**.

35 N. Sharma, *et al.*, High-Resolution AlGaN/GaN HEMT-Based Electrochemical Sensor for Biomedical Applications, *IEEE Trans. Electron Devices*, 2020, **67**(1), 289–295, DOI: **10.1109/TED.2019.2949821**.

36 S. Mishra and N. Chaturvedi, Simulation and machine learning modelling based comparative study of InAlGaN and Al-GaN high electron mobility transistors for the detection of HER-2, *Anal. Methods*, 2021, **13**, 3659–3666, DOI: **10.1039/D1AY00707F**.

37 P. Kachhawa, *et al.*, Antigen-Antibody Interaction-Based GaN HEMT Biosensor for C3G Detection, *IEEE Sens. J.*, 2022, **22**(7), 6256–6262, DOI: **10.1109/JSEN.2022.3150027**.

38 P. Kachhawa, S. Mishra, A. K. Jain, R. R. Thakur and N. Chaturvedi, 200 V-Depletion mode GaN HEMT on Si, *2020 5th IEEE International Conference on Emerging Electronics (ICEE)*, 2020, pp. 1–4, DOI: **10.1109/ICEE50728.2020.9776649**.

39 J. C. Love, L. A. Estroff, J. K. Kriebel, R. G. Nuzzo and G. M. Whitesides, Self-Assembled Monolayers of Thiolates on Metals as a Form of Nanotechnology, *Chem. Rev.*, 2005, **105**(4), 1103–1170, DOI: **10.1021/cr0300789**.

40 Y. Xue, X. Li, H. Li and W. Zhang, Quantifying thiol-gold interactions towards the efficient strength control, *Nat. Commun.*, 2014, **5**, 4348, DOI: **10.1038/ncomms5348**.

41 Q. Yan, H. N. Zheng, C. Jiang, K. Li and S. J. Xiao, EDC/NHS activation mechanism of polymethacrylic acid: Anhydride versus NHS-ester, *RSC Adv.*, 2015, **5**(86), 69939–69947, DOI: **10.1039/c5ra13844b**.

42 E. Y. Liu, S. Jung and H. Yi, Improved Protein Conjugation with Uniform, Macroporous Poly(acrylamide-coacrylic acid) Hydrogel Microspheres via EDC/NHS Chemistry, *Langmuir*, 2016, **32**(42), 11043–11054, DOI: **10.1021/acs.langmuir.6b02591**.

43 S. Wang, N. Mamedova, N. A. Kotov, W. Chen and J. Studer, Antigen/Antibody Immunocomplex from CdTe Nanoparticle Bioconjugates, *Nano Lett.*, 2002, **2**(8), 817–822, DOI: **10.1021/nl0255193**.

44 B. Varnholt, P. Oulevey, S. Luber, C. Kumara, A. Dass and T. Burgi, Structural information on the Au-S interface of thiolate-protected gold clusters: A raman spectroscopy study, *J. Phys. Chem. C*, 2014, **118**(18), 9604–9611, DOI: **10.1021/jp502453q**.

45 Z. Zhang and M. Lin, Fast loading of PEG-SH on CTABprotected gold nanorods, *RSC Adv.*, 2014, **4**(34), 17760–17767, DOI: **10.1039/c3ra48061e**.

46 T. Burgi, Properties of the gold-sulphur interface: from selfassembled monolayers to clusters, *Nanoscale*, 2015, **7**(38), 15553–15567, DOI: **10.1039/c5nr03497c**.

47 S. Aryal, B. K. C. Remant, N. Dharmaraj, N. Bhattarai, C. H. Kim and H. Y. Kim, Spectroscopic identification of SAu interaction in cysteine capped gold nanoparticles, *Spectrochim. Acta, Part A*, 2006, **63**(1), 160–163, DOI: **10.1016/j.saa.2005.04.048**.

48 B. R. Khalkho, *et al.*, Citrate functionalized gold nanoparticles assisted micro extraction of L-cysteine in milk and water samples using Fourier transform infrared spectroscopy, *Spectrochim. Acta, Part A*, 2022, **267**, 120523, DOI: **10.1016/J.SAA.2021.120523**.

49 N. K. M. Churcher, S. Upasham, P. Rice, S. Bhadsavle and S. Prasad, Development of a flexible, sweat-based neuropeptide y detection platform, *RSC Adv.*, 2020, **10**(39), 23173–23186, DOI: **10.1039/d0ra03729j**.

50 C. Branca, *et al.*, Role of the OH and NH vibrational groups in polysaccharide-nanocomposite interactions: A FTIR-ATR study on chitosan and chitosan/clay films, *Polymer*, 2016, **99**, 614–622, DOI: **10.1016/j.polymer.2016.07.086**.

51 A. Krolikowska, A. Kudelski, A. Michota and J. Bukowska, SERS studies on the structure of thioglycolic acid monolayers on silver and gold, *Surf. Sci.*, 2003, 227–232, DOI: **10.1016/S0039-6028(03)00094-3**.

52 V. Agnolon, *et al.*, ELISA assay employing epitope-specific monoclonal antibodies to quantify circulating HER2 with potential application in monitoring cancer patients undergoing therapy with trastuzumab, *Sci. Rep.*, 2020, **10**(1), 1–12, DOI: **10.1038/s41598-020-59630-y**.

53 B. Armstrong, Antigen–antibody reactions, *ISBT Sci. Ser.*, 2008, **3**, 21–32, DOI: **10.1111/j.1751-2824.2008.00185.x**.

54 M. Samae, S. Chatpun and S. Chirasatitsin, Hemagglutination Detection with Paper-Plastic Hybrid Passive Microfluidic Chip, *Micromachines*, 2021, **12**(12), 1533, DOI: **10.3390/mi12121533**.

55 N. Ayawei, A. N. Ebelegi and D. Wankasi, Modelling and Interpretation of Adsorption Isotherms, *J. Chem.*, 2017, **2017**, 3039817, DOI: **10.1155/2017/3039817**.

56 K. Jayant, K. Auluck, S. Rodriguez, Y. Cao and E. C. Kan, Programmable ion-sensitive transistor interfaces. III. Design considerations, signal generation, and sensitivity enhancement, *Phys. Rev. E: Stat., Nonlinear, Soft Matter Phys.*, 2014, **89**(5), 1–12, DOI: **10.1103/PhysRevE.89.052817**.

57 M. Belter, A. Sajnog and D. Barałkiewicz, Over a century of detection and quantification capabilities in analytical chemistry—Historical 553 overview and trends, *Talanta*, 2014, **129**, 606–616, DOI: **10.1016/j.talanta.2014.05.018**.

58 D. H. Kim, S. M. Seo, S. H. Paek, G. S. Lim and S. H. Paek, Premature antibodies with rapid reaction kinetics and their characterization for diagnostic applications, *Anal. Biochem.*, 2012, **420**(1), 54–60, DOI: **10.1016/j.ab.2011.09.006**.

59 K. Mitsakakis and E. Gizeli, Multi-sample acoustic biosensing microsystem for protein interaction analysis, *Biosens. Bioelectron.*, 2011, **26**(11), 4579–4584, DOI: **10.1016/j.bios.2011.05.030**.

60 L. S. Jung, K. E. Nelson, P. S. Stayton and C. T. Campbell, Binding and dissociation kinetics of wild-type and mutant streptavidins on mixed biotin-containing alkylthiolate monolayers, *Langmuir*, 2000, **16**(24), 9421–9432, DOI: **10.1021/la000144r**.

61 G. K. Joshi, S. Deitz-McElyea, T. Liyanage, K. Lawrence, S. Mali, R. Sardar and M. Korc, *ACS Nano*, 2015, **9**(11), 11075–11089, DOI: **10.1021/acsnano.5b04527**.

62 S. Myung, A. Solanki, C. Kim, J. Park, K. S. Kim and K. B. Lee, Grapheneencapsulated nanoparticle-based biosensor for the selective detection of cancer biomarkers, *Adv. Mater.*, 2011, **23**(19), 2221–2225, DOI: **10.1002/adma.201100014**, Epub 2011 Apr 5, PMID: 21469221; PMCID: PMC3181002.

